

PapRIV, a BV-2 microglial cell activating quorum sensing peptide.

Yorick Janssens¹, Nathan Debunne¹, Anton De Spiegeleer^{1,2,3}, Evelien Wynendaele¹, Marta Planas⁴,
Lidia Feliu⁴, Alessandra Quarta^{5,6}, Christel Claes⁷, Debby Van Dam^{8,9}, Peter Paul De Deyn^{8,9}, Peter
Ponsaerts^{5,6}, Matthew Blurton-Jones^{7,10,11} and Bart De Spiegeleer^{1*}.

¹ Drug Quality and Registration (DruQuaR) group, Faculty of Pharmaceutical Sciences, Ghent University, Ghent, Belgium.

² Department of Geriatrics, Faculty of Medicine and Health Sciences, Ghent University Hospital, Ghent, Belgium

³ Unit for Molecular Immunology and Inflammation, VIB-Center for Inflammation Research, Zwijnaarde, Belgium

⁴ LIPPSO, University of Girona, Girona, Spain.

⁵ Laboratory of Experimental Hematology, University of Antwerp, Wilrijk, Belgium

⁶ Vaccine and Infectious Disease Institute (Vaxinfectio), University of Antwerp, Wilrijk, Belgium.

⁷ Sue and Bill Gross Stem Cell Research Center, University of California, Irvine, CA 92696, USA.

⁸ Laboratory of Neurochemistry and Behavior, Institute Born-Bunge, University of Antwerp, Wilrijk, Belgium

⁹ Department of Neurology and Alzheimer Center, University of Groningen, University Medical Center Groningen, Groningen, the Netherlands.

¹⁰ Department of Neurobiology & Behavior, University of California, Irvine, CA 92697, USA

¹¹ Institute for Memory Impairments and Neurological Disorders, University of California, Irvine, CA 92696, USA

* Corresponding author: Tel: +32 9 264 81 00; Fax: +32 9 264 81 93; *E-mail address*:

Bart.DeSpiegeleer@UGent.be.

(*O/Ref. 2020-137d*)

24 **Abstract**

25 **Background**

26 Quorum sensing peptides (QSPs) are bacterial peptides produced by Gram-positive bacteria to
27 communicate with their peers in a cell-density dependent manner. These peptides do not only
28 act as interbacterial communication signals, but can also have effects on the host. Compelling
29 evidence demonstrates the presence of a gut-brain axis and more specifically, the role of the gut
30 microbiota in microglial functioning. The aim of this study is to investigate microglial
31 activating properties of a selected QSP (PapRIV) which is produced by *Bacillus cereus* species.

32 **Methods**

33 Gastro-intestinal transport of the peptide is investigated using the *in vitro* Caco-2 model while
34 transport over the blood-brain barrier is investigated in mice using multiple time regression
35 experiments. Microglial activation is assessed using ELISA, fluorometry, immunoblotting,
36 qPCR and phase-contrast microscopy. *In vivo* plasma detection and *ex vivo* metabolization
37 experiments are performed using UHPLC-MS² and UHPLC-UV/MS, respectively.

38 **Results**

39 PapRIV showed *in vitro* activating properties of BV-2 microglia cells and was able to cross the
40 *in vitro* Caco-2 cell model and pass the blood-brain barrier *in vivo*. *In vivo* peptide presence was
41 also demonstrated in mouse plasma. The peptide caused induction of IL-6, TNF α and ROS
42 expression and increased the fraction of amoeboid BV-2 microglia cells in an NF- κ B dependent
43 manner. Different metabolites were identified in serum, of which the main metabolite
44 (DLPEFH) still remained active.

45 **Conclusions**

46 PapRIV is thus able to cross the gastro-intestinal tract and the blood-brain barrier and shows *in*
47 *vitro* activating properties in BV-2 microglia cells, hereby indicating a potential role of this
48 quorum sensing peptide in gut-brain interaction.

49 **Keywords:** Quorum sensing, peptide, microglia, BV-2, PapRIV, neuro-inflammation, *Bacillus*
50 *cereus*

51 **Background**

52 Quorum sensing is a cell-cell communication system used by micro-organisms to sense the
53 density of their peers by secreting quorum sensing molecules. By using this system, gene
54 expression is regulated in response to the microbial cell density. A variety of cell functions such
55 as expression of virulence factors, biofilm formation, competence and sporulation are
56 controlled by this communication system [1]. The process of quorum sensing is not only limited
57 to bacteria, but it is also observed in other microbial cell types such as yeasts and fungi [2, 3].
58 Different types of quorum sensing molecules in bacteria exist: Gram-negative bacteria mostly
59 use N-acyl homoserine lactones, while Gram-positive bacteria produce oligopeptides for their
60 communication, which are called quorum sensing peptides (QSPs) [4-6]. Other quorum sensing
61 molecules, such as furan borate derivatives and other miscellaneous molecules, exist as well [7,
62 8]. The QSPs are produced as large pro-peptides, secreted outside the microbial cell by ATP-
63 binding cassette transporters, whilst hydrolyzed to the active QSP. They then interact with
64 neighboring microbial cells via two possible mechanisms: either with membrane-located
65 receptors (mainly histidine kinases) for signal transduction, or directly with cytoplasmic sensors
66 (*e.g.* the RNPP family) after being transported over the microbial cell membrane by
67 oligopeptide permeases [4]. The QSPs are chemically and microbiologically described in the
68 Quorumpeps[®] database which currently contains over 350 different peptides [9]. Recently, it
69 has been found that these peptides not only influence micro-organisms but can also affect cells
70 of the host. For example, QSPs promote tumor cell invasion and angiogenesis *in vitro*, thereby
71 promoting epithelial-mesenchymal transition and metastasis [10, 11]. The human immune
72 system also makes use of these molecules for controlling infection. Mast cells are able to sense
73 CSP-1, a QSP produced by *Streptococcus pneumoniae*, hereby triggering degranulation and the
74 release of antibacterial mediators [12]. *In vitro* research also suggests that QSPs influence host
75 muscle wasting diseases [13]. QSPs can cross the blood-brain barrier and thus potentially

76 influence brain cells [14]. Indeed, an *in vitro* screening of 85 different QSPs indicated that some
77 peptides have the ability to exert biological effects on different types of brain cells [15].
78 Microbial dysbiosis is observed in a variety of neurodevelopmental-, neurodegenerative- and
79 psychiatric disorders such as autism spectrum disorders (ASD), schizophrenia, Alzheimer's
80 disease (AD), major depressive disorder, and Parkinson's disease (PD) [16-24]. A causal
81 relationship between these gut microbiota and brain disorders is becoming increasingly evident:
82 fecal transfer of human ADHD, PD and AD patients aggravates symptoms in *in vivo* mice
83 models of these disorders [25-27]. Alternatively, transfer of a 'healthy' microbiota reduced
84 amyloid and tau pathology in an AD mouse model [28]. This microbiota-brain association is
85 considered part of a bi-directional communication pathway between the gut and brain, called
86 the gut-brain axis [29]. Various communication routes including the immune system, the vagus
87 nerve, the enteric nervous system and microbial metabolites, such as short chain fatty acids,
88 amino acids and peptidoglycans are proposed as mediators of this axis, but many factors remain
89 largely unknown [30]. Peptides also contribute in this microbiome-to-brain signaling as
90 interactions of the microbiota with gut hormones and entero-endocrine peptides are observed
91 [31]. Microglial dysfunction and activation is present in a variety of neuronal conditions such
92 as AD, ASD, multiple sclerosis, PD and amyotrophic lateral sclerosis [25, 32-37]. Germ-free
93 mice display global defects in microglia with altered cell proportion and an immature
94 phenotype, indicating that the gut microbiome plays a role in microglial maturation and
95 functioning during development and aging [32, 38]. When transplanting faeces from human
96 AD or PD patients to *in vivo* mouse models, cognitive and physical impairments are aggravated,
97 which is partly mediated by enhanced microglial activation in the brain [25, 26]. Prebiotics are
98 already being developed that target this gut microbiota-microglial axis for the treatment of AD.
99 Sodium oligomannate, which will shortly be studied as an investigational drug in a large AD
100 phase III global clinical trial, suppresses gut dysbiosis together with the associated

101 phenylalanine/isoleucine accumulation in an AD mouse model, resulting in reduced microglial
102 activation, amyloid- β deposition, tau phosphorylation and amelioration of cognitive
103 impairment [39]. All these studies indicate that the gut microbiota can influence
104 neurodevelopmental-, neurodegenerative- and psychiatric disorders by regulation of microglia
105 cells. However, the exact mechanisms on how the gut microbiota influence these microglial
106 cells remains largely unknown.

107 PapRIV is a heptapeptide (SDLPFEH) originating from the *Bacillus cereus* group, which
108 comprises a number of highly related species. The *B. cereus* group (sensu lato), which is
109 widespread in soil and food, is generally considered as an opportunistic human pathogen
110 because it triggers food-borne gastroenteritis and some non-gastro-intestinal infections like
111 pneumonia and endophthalmitis, as well as infections resembling to anthrax. However,
112 presence of *B. cereus* in the human gastro-intestinal tract is already been demonstrated without
113 provoking illness, indicating the symbiotic life cycle of this species [40]. The diseases
114 associated with *B. cereus* are caused by several cytotoxic products, which are produced by
115 activation of the PlcR quorum sensing system. The PapRIV peptide is translated as a 48- amino
116 acid polypeptide which is secreted out of the cell under influence of the N-terminal signaling
117 sequence and extracellularly processed by NprB proteases to form the active PapRIV
118 heptapeptide [41, 42]. Instead of binding to a membrane-coupled sensor receptor and activating
119 a two-component signaling system, PapRIV binds directly to its regulatory cytoplasmatic PlcR
120 protein after being imported in the cell by the ABC transporter family member Opp
121 (oligopeptide permease). This binding activates the regulatory PlcR protein resulting in a
122 conformational change, binding to the promotor region and transcriptional activation of PlcR
123 target genes [43, 44]. Activation of this quorum sensing system induces production of
124 extracellular virulence factors, such as enterotoxins, haemolysins, cytotoxins and various
125 degradative enzymes (*e.g.* proteases). However, the effects of the peptide itself towards the host

126 remains unexplored. Here, we demonstrate for the first time microglial activating properties of
127 a QSP, indicating the potential of these peptides as mediators of the gut-brain-microglia axis.

128 **Methods**

129 **Peptides and Reagents**

130 Synthetic PapRIV was purchased from GL Biochem (Shanghai, China). The alanine scan,
131 metabolites and scrambled control were synthesized using solid-phase peptide synthesis
132 (Supplementary method S1). The quality of all peptides was determined using an in-house
133 developed QC method and a purity of 95% or more was found for each sequence. Calcium
134 dichloride dihydrate, magnesium sulphate, potassium chloride, sodium dihydrogen phosphate
135 hydrate, HEPES, sodium lactate and urethane were purchased from Sigma-Aldrich (Diegem,
136 Belgium), while Bovine Serum Albumin (BSA), sodium iodide, sodium dihydrogen phosphate
137 monohydrate were obtained from Merck KGaA (Darmstadt, Germany). Sodium chloride and
138 disodium hydrogen phosphate dihydrate were obtained from VWR (Leuven, Belgium).
139 Calcium dichloride and D-glucose were purchased from Fluka (Diegem, Belgium) and dextran
140 from AppliChem GmbH (Darmstadt, Germany). Water was purified using an Arium 611 Pro
141 VF purification system (Sartorius, Göttingen, Germany) to laboratory-graded water (18.2 M Ω
142 \times cm).

143 **Animals**

144 Female, Institute for Cancer Research, Caesarean Derived-1 (ICR-CD-1) mice (Envigo,
145 Venray, The Netherlands) of age 7-10 weeks and weighing 26-30 g, were used during the blood-
146 brain barrier (BBB) transport experiments and C57Bl6/J WT mice, aged 3-24 months, were
147 used for detection of PapRIV in plasma. Feed and water were provided ad libitum. All animal
148 experiments were performed in strict accordance with the Belgian legislation RD 31/12/2012
149 and the Ethical Committee principles of laboratory animal welfare; the protocols were approved

150 by the Ethical Committee of Ghent University, Faculties of Veterinary Medicine and Medicine
151 and Health Sciences (approval numbers 2014-128 and ECD 19-17).

152 **Cells**

153 BV-2 cells were a kind gift from Prof. Alba Minelli and were grown in RPMI medium
154 supplemented with 10% fetal bovine serum (FBS) and 1% penicillin-streptomycin solution
155 (Life Technologies, Belgium). The cells were cultured in culture flasks (Greiner, Belgium) in
156 an incubator set at 37°C and 5% CO₂. When confluent, cells were detached using a cell scraper
157 and diluted 1:20 approximately every 4 days. Experiments were performed in serum-free
158 DMEM without phenol red.

159 SH-SY5Y neuroblast cells (Sigma-Aldrich, Diegem, Belgium) were grown in F12:MEM
160 (50/50 v/v) medium supplemented with 15% FBS, 1% non-essential amino acids (NEAA),
161 2mM L-Glutamine and 1% penicillin/streptomycin solution (Life Technologies, Belgium) in an
162 incubator set at 37°C and 5% CO₂. When confluent, cells were detached using 0.25% Trypsin-
163 EDTA.

164 **Caco-2 assay**

165 Caco-2 cells were grown in DMEM supplemented with 10% FBS, 1% NEAA and 1%
166 penicillin/streptomycin solution. A total of 3×10^5 cells per filter were seeded in a 12-well plate
167 and left for differentiation during 21-29 days (medium change every other day). Monolayer
168 formation was checked by measuring the TEER values which should be above $0.30 \text{ k}\Omega \times \text{cm}^2$
169 [45]. After washing with Hank's balanced salt solution, 400 μL of a 1 μM peptide solution was
170 added to the apical side of the filter. After 30, 60, 90 and 120 minutes, 100 μL of the acceptor
171 compartment was taken for UPLC-MS/MS analysis (Supplementary method S2). Linear curve
172 fitting was used to calculate the apparent permeability coefficient (P_{app}), as sink conditions were

173 achieved. The P_{app} was determined from the amount of peptide transported per time unit and
174 calculated using the following equation:

$$175 \quad P_{app} = \left(\frac{dQ}{dt} \right) \times \left(\frac{1}{A \times C_0} \right) \quad (1)$$

176 with dQ/dt = the steady-state flux (pM/s), experimentally obtained

177 A = the surface area of the filter (= 1.12 cm²)

178 C_0 = the initial concentration in the donor compartment (= 1 x 10⁶ pM)

179 The reduction in acceptor concentration was also taken into account after every sampling. The
180 cumulative amount in the acceptor compartment is defined as:

$$181 \quad \text{Cumulative amount} = C_{r_n} V_r + \sum_{k=1}^{n-1} C_{r_k} V_s \quad (2)$$

182 with C_{r_k} = concentration at sample point k in acceptor compartment

183 V_r = volume in the receiver chamber

184 V_s = volume sampled

185 n = times sampled

186 **Detection of PapRIV in mouse plasma**

187 Sixty μ L of mouse plasma was used for the detection of PapRIV and prepared using solid-phase
188 extraction (SPE). Mouse plasma was mixed with an ACN/DMSO mixture acidified with FA
189 (94/3/3 V/V). After 30s vortexing and sonification (30s), the sample was boiled for 1min at
190 100° followed by centrifugation (30s, 10,000g). One hundred μ L of the supernatant was then
191 mixed with 800 μ L ACN/DMSO mixture (97/3 V/V) acidified with 0.1% FA. This sample was
192 then loaded on a MonoSpin Amide SPE column (GL Sciences Inc., Japan) conditioned with a
193 water/ACN mixture (90/10 V/V) basified with 0.1% NH₄OH and equilibrated with the same

194 ACN/DMSO mixture. The sample was eluted using a water/ACN/DMSO mixture (75/20/5
195 V/V) acidified with 0.1% FA. The eluent was brought into vials which were coated with an
196 albumin based anti-adsorption solution, which considerably decreases the adsorption to glass
197 for certain peptides and improves the overall sensitivity of the method [46]. Ten μL of the eluent
198 was injected on an Acquity UPLC® BEH C18 (2.1 x 100 mm; 1.7 μm) column equipped with
199 a guard column. Column temperature was maintained at 60°C. Mobile phase A consisted of
200 water/ACN/DMSO (93/2/5 V/V) + 0.1% FA, Mobile phase B consisted of water/ACN/DMSO
201 (2/93/5 V/V) + 0.1% FA. A gradient ranging from 100% mobile phase A to 60% mobile phase
202 B over 12 minutes was used. MS analysis was performed using a Quadrupole-Time-of-flight
203 system (SYNAPT G2-Si) (Waters, Milford, USA). The SYNAPT G2-Si with electrospray
204 ionisation was set in positive mode. Ionization was conducted using a needle voltage of 3.0 kV,
205 a cone voltage of 20 V and a source temperature of 120°C. Nitrogen was used as sheath and
206 auxiliary gas at a temperature of 500°C. Argon was used as collision gas at an energy of 32 V.
207 Detection was performed using a fixed mass and collision energy on the first quadrupole set on
208 the mother ion ($844.35 \pm 0.5 m/z$) and MS/MS acquisition over the 100-1450 m/z range using
209 the second TOF analyser. Samples were considered positive when a signal appeared at the
210 expected retention time ($\Delta < 1\%$) and when at least three identification ions (one parent ion and
211 two daughter ions) of the peptide were found [47].

212 **Peptide ^{125}I radiolabelling**

213 PapRIV and the controls BSA and dermorphin (Hanhong, Shanghai, China) were iodinated
214 using the Iodo-Gen® method as previously described [48]. Briefly, 0.1 μmol of the lyophilized
215 peptide was dissolved in 100 μL of phosphate buffer (pH 7.4, 25 mM). A Iodo-Gen® coated
216 tube (Thermo Scientific, Merelbeke, Belgium) was first of all rinsed with 1 mL of phosphate
217 buffer. Subsequently, 50 μL of sodium iodide solution (1.1 $\mu\text{mol}/\text{mL}$) and 1 mCi of Na^{125}I
218 solution (Perking Elmer, Zaventem, Belgium) were transferred into this Iodo-Gen® coated

219 tube. The oxidation reaction was allowed to proceed for six minutes at room temperature, after
220 which the iodonium solution was transferred to 50 μ L of peptide solution (1 mM). The
221 iodination reaction of the peptide was allowed to proceed for another six minutes at room
222 temperature. Finally, the iodinated peptide was purified using a silver filter (Thermo Scientific,
223 Merelbeke, Belgium).

224 **Multiple time regression analysis**

225 In order to determine whether the peptide could enter the brain, *in vivo* multiple time regression
226 (MTR) analysis was performed. ICR-CD-1 mice were anesthetized intraperitoneally using a
227 40% urethane solution (3 g/kg). Then, the jugular vein and carotid artery were isolated and 200
228 μ L of the radiolabeled peptide solution, diluted to 30,000 cpm/ μ L using Lactated Ringer's
229 solution containing 1% of BSA (LR/BSA), was injected into the jugular vein. At specified time
230 points after injection (i.e. 1, 3, 5, 10, 12.5 and 15 min, with start and end in duplicate), blood
231 was obtained from the carotid artery followed by decapitation of the mouse. The isolated brain
232 was weighed and radioactivity measured in a gamma counter for 5 minutes (Wallac Wizard
233 automatic gamma counter, Perkin Elmer, Shelton, CT, USA), as well as from 50 μ L serum,
234 which was obtained by centrifuging the collected blood at 10,000 g for 15 min at 21°C. The
235 linear and biphasic modeling of the multiple time regression analysis was performed as
236 previously described [14].

237 **Capillary depletion**

238 We performed capillary depletion to determine whether the peptides, taken up by the brain,
239 completely crossed the capillary wall into the tissue rather than just being trapped by and in the
240 endothelium. The method of Triguero *et al.*, as modified by Gutierrez *et al.*, was used [49, 50].
241 ICR-CD-1 mice were first anesthetized intraperitoneally using a 40% urethane solution (3
242 g/kg). After isolation of the jugular vein, 200 μ L of the iodinated peptide solution, diluted to 10

243 000 cpm/ μ L using LR/BSA, was injected in the jugular vein. Ten minutes after injection, blood
244 was collected from the abdominal aorta and the brain was perfused manually with 20 mL of
245 Lactated Ringer's buffer after clamping the aorta and severing the jugular veins. Subsequently,
246 the brain was collected, weighed and the radioactivity measured in the gamma counter for 5
247 minutes. Then, the brain was homogenized with 0.7 mL of ice-cold capillary buffer (10 mM
248 HEPES, 141 mM NaCl, 4 mM KCl, 2.8 mM CaCl₂, 1 mM MgSO₄, 1 mM NaH₂PO₄ and 10
249 mM D-glucose adjusted to pH 7.4) in a pyrex glass tube and mixed with 1.7 mL of 26% ice-
250 cold dextran solution in capillary buffer. The resulting solution was weighed and centrifuged
251 in a swinging bucket rotor at 5,400 g for 30 min at 4°C, after measuring the radioactivity in the
252 gamma counter. Pellet (capillaries) and supernatant (parenchyma and fat tissues) were also
253 collected, weighed and measured in a gamma counter. After centrifuging the obtained blood
254 (10,000 g, 21°C, 15 min), the radioactivity of 50 μ L serum was measured in a gamma counter
255 as well.

256 **Brain-to-blood transport**

257 We quantified the amount of peptide exported out of the brain as previously described [51].
258 ICR-CD-1 mice were anesthetized intraperitoneally using a 40% urethane solution (3 g/kg).
259 Then, the skin of the skull was removed and using a 22 G needle marked with tape at 2 mm, a
260 hole was made into the lateral ventricle at the following coordinates: 1 mm lateral and 0.34 mm
261 posterior to the bregma. The anesthetized mice received an intracerebroventricular (ICV)
262 injection of 1 μ L of the diluted iodinated peptide solution using LR/BSA (25,000 cpm/ μ L) by
263 pumping the peptide solution at a speed of 360 μ L/h for 10 s using a syringe pump (KDS100,
264 KR analytical, Cheshire, UK). At specified time points after ICV-injection (i.e. 1, 3, 5, 10, 12.5
265 and 15 min), blood was collected from the abdominal aorta and subsequently the mouse was
266 decapitated. Then, the whole brain was collected, weighed and measured in a gamma counter
267 for 5 minutes. Fifty μ L of serum, which was obtained by centrifuging the collected blood at 10

268 000 g during 15 min at 21°C, and the background was also measured in a gamma counter. The
269 efflux half-life was calculated from the linear regression of the natural logarithm of the residual
270 radioactivity in brain versus time as follows:

$$271 \quad t_{1/2} = \frac{\ln(2)}{k_{out}} \quad (3)$$

272 where k_{out} is defined as the efflux rate constant calculated as the negative value of the slope of
273 the linear regression, applying first order kinetics.

274 **IL-6 and TNF α determination**

275 To investigate the microglia activating properties of the peptide, IL-6 and TNF α levels were
276 determined in cell-free supernatants of BV-2 microglia cells after treatment. BV-2 cells (2 x
277 10⁵ cells/well) were seeded in 24-well plates and treated with peptide for 20 hours. ELISA was
278 performed according to the supplier's protocol (eBioscience, Vienna, Austria). Briefly, after
279 incubation with biotinylated detection antibody, avidin-HRP conjugate and subsequently
280 chromogenic tetramethylbenzidine (TMB) substrate were added. Absorbance was measured at
281 450 nm and 570 nm using the Multiskan Ascent 354 microplate reader (Thermofisher,
282 Waltham, USA). Concentrations were determined using the standard curve generated using
283 known concentrations of TNF α and IL-6.

284 **qPCR**

285 To confirm the observed ELISA results at mRNA level, a qPCR experiment was performed.
286 After incubation of the BV-2 cells with PapRIV or controls, cells were lysed in RLT buffer
287 (Qiagen, Hilden, Germany) supplemented with 1% β -mercaptoethanol. The lysate was stored
288 at -80°C until RNA extraction. RNA was extracted using the RNeasy Mini Kit (Qiagen, Hilden,
289 Germany). DNase steps were included in the protocol to remove possible DNA contamination.
290 RNA purity and concentration were assessed using spectrophotometry (NanoDrop), while RNA

291 quality was evaluated using capillary electrophoresis (Fragment Analyzer). After extraction,
292 the RNA was immediately converted to cDNA which was stored at -20°C until qPCR analysis.
293 Ppia and Rer were chosen as suitable control genes based on the GeNorm and Normfinder
294 algorithms [52, 53]. Used primers are given in Table 1. qPCR cycling was performed using a
295 LightCycler 480 (Roche), with Cq values being calculated using the second derivative threshold
296 method.

297 **Table 1: Primers for BV-2 qPCR**

Gene	Supplier	Sequence (5' → 3')
IL-6	Invitrogen	Fw: ACCACTTCACAAGTCGGAGGC Rev: CTGCAAGTGCATCATCGTTGTTC
Ppia	Qiagen	- ¹
Rer	Invitrogen	Fw: AGTGGATCCTTCCTTGATGG Rev: ATGCCTTTTGTAGCTGCG

298 ¹ Sequence of the primers is not disclosed by Qiagen.

299 **ROS assay**

300 Microglia activation is accompanied by an increased reactive oxygen species (ROS)
301 production. The ROS assay was performed using a fluorometric intracellular ROS kit according
302 to the supplier's protocol (Sigma-Aldrich, Diegem, Belgium). In brief, 4 x 10⁴ cells/well were
303 seeded in a black 96-well plate. Four hours post seeding, 100 µL of master reaction mix was
304 added to the wells and incubated for 1 h after which cells were treated with PapRIV dissolved
305 in PBS for 24h. Fluorescence intensity was measured using an EnVision fluorometric plate
306 reader at $\lambda_{\text{ex}} = 492/\lambda_{\text{em}} = 535$ nm (Perkin Elmer, Zaventem, Belgium).

307 **Morphological analysis**

308 We investigated the morphology since microglia change their morphology from a branched
309 structure to a more round, ameboid structure after activation. BV-2 cells were seeded in 1 x 10⁴
310 cells/well in a 24-well plate (360 µL); this way direct cell-cell contacts, which have an influence
311 on morphology, are avoided. Four hours post-seeding, cells were treated with 40 µL peptide,
312 placebo (H₂O), medium or positive control (LPS 1 µg/mL). For the assessment of the

313 morphology, one picture in the center of each well (100x magnification) was taken after twenty
314 hours with an Olympus CKX53 phase-contrast microscope equipped with an XC30 CCD
315 camera (Olympus NV, Antwerp, Belgium). The number of branched and ameoboid cells was
316 counted with the cell counter plugin of ImageJ.

317 **Immunoblotting**

318 To assess nuclear translocation of NF- κ B, cells were lysed after 20h using the NE-PER™
319 protocol (Thermo Scientific). Using this kit, the cytoplasmic and nuclear protein fractions are
320 separated from each other. To asses I κ B α expression, cells were lysed with RIPA buffer. Protein
321 content of the lysates was determined using the modified Lowry assay (Thermo Scientific).
322 Proteins (20 μ g) were separated using an Any kD gel (SDS-PAGE) and transferred to a
323 nitrocellulose membrane (BioRad, Temse, Belgium). Aspecific binding sites were blocked for
324 30 min using TBS + 1% casein (BioRad, Temse, Belgium). Western blot was performed using
325 the following primary antibodies overnight (4°C): anti-p65 NF κ B (1/500), anti-I κ B α (1/1000)
326 and anti- β -actin (1/1000), β -tubulin (1/4000) and anti-Histon H3.3 (1/5000) were used as
327 loading controls. Goat anti-rabbit-AP antibody was used for detection (1/10000) (60 min). All
328 antibodies were purchased at Thermo Scientific (Merelbeke, Belgium). Finally, the BCIP/NBT
329 substrate was added and the results were analyzed using the GelDoc EZ imager and Image Lab
330 software (BioRad, Temse, Belgium). TBS buffer was used for washing between the steps.

331 **MTT assay**

332 SH-SY5Y cells were seeded at a density of 5×10^4 cells/well in a 96-well plate and incubated
333 for 24 h. Next, medium was removed and replaced by 200 μ L conditioned medium of BV-2
334 cells which were treated for 20 h with PapRIV. After 24 h incubation, 20 μ L MTT reagent
335 (12mM) was added and incubated for 3 h. Finally, the medium was removed and replaced by

336 150 μ L DMSO and measured at 570 nm with a microplate reader (Thermofisher, Waltham,
337 USA).

338 **Ex vivo metabolism**

339 Peptide solution (0.1 mg/mL) was incubated with serum, brain, liver, kidney or faeces
340 homogenate at 37°C. After 0, 5, 10, 30 and 60 minutes, aliquots were taken for UPLC-UV/MS
341 analysis. Preparation of the tissue homogenates and UPLC-UV/MS parameters are given in
342 supplementary information (Supplementary methods S3-S4). The half-life was calculated
343 using the following equation:

$$344 \quad T_{1/2} = \frac{-\ln(2)}{\text{Slope}} \quad (4)$$

345 Where the slope is defined by linear regression assuming first order kinetics.

346 **Statistical analysis**

347 Statistical analysis of PapRIV treated cells compared to vehicle treated cells was performed
348 using one-way ANOVA; the Dunnett test was performed to adjust for multiple comparisons
349 with the control group (placebo). A p-value of <0.05 was considered significant. The Mann-
350 Whitney U test was used for the qPCR experiment. Linear and biphasic modelling was applied
351 for the MTR experiments as described by Wynendaele *et al.* [14]. For the efflux and Caco-2
352 experiment, regular linear regression was applied. Data are expressed as mean \pm SEM unless
353 otherwise specified. Statistical analysis was performed and graphs were made using Graphpad
354 Prism 6 (Graphpad Software, La Jolla, USA).

355 **Results**

356 **PapRIV is able to reach the circulation and cross the blood-brain barrier**

357 PapRIV showed a low transport rate across the Caco-2 monolayer with a P_{app} of $1.37 \pm 0.21 \times$
358 10^{-9} cm/s and is thus potentially able to cross the intestinal wall and reach the circulation (Figure

359 1a). Indeed, PapRIV was detected in 4 out of 66 wild type mice plasma samples (Table 2 and
360 Supplementary Fig. S1) which is an extra indication that the peptide is able to cross the gastro-
361 intestinal tract and reach the circulation *in vivo*. Once circulating, the peptide is able to cross
362 the blood-brain barrier based on experiments in the *in vivo* MTR mice model (Figure 1b). The
363 pharmacokinetic parameters of PapRIV and of the negative and positive control, respectively
364 BSA and Dermorphin, are given in Table 3. BSA and Dermorphin followed a linear model
365 while the PapRIV peptide displayed a biphasic model with an initial steep influx followed by a
366 steady state situation. PapRIV showed an initial brain influx rate (K_i) of $6.95\mu\text{l}/(\text{g} \times \text{min})$ and
367 can be classified as a peptide with a very high brain influx according to the classification system
368 designed by Stalmans *et al.* [54]. Based on the capillary depletion experiment, it was observed
369 that 87% of the peptide that is taken up by the brain eventually reached the parenchyma (Figure
370 1c and Table 3). Once the peptide enters the brain, no efflux back to the circulation is observed
371 as the k_{out} was not significantly different from zero (Figure 1d and Table 3). In conclusion, the
372 peptide is able to pass the Caco-2 monolayer, can be detected in mouse plasma and is able to
373 pass the blood-brain barrier and reach the brain where possible effects can be exerted.

374 **Table 2: Measured parent- and daughter ions in positive mice plasma samples.**

Samples	Parent ions			Daughter ions		
	Theoretical (<i>m/z</i>) ¹	Measured (<i>m/z</i>)	Δ^2	Theoretical (<i>m/z</i>) ³	Measured (<i>m/z</i>)	Δ^2
Sample 6	844.3836	844.3639	+0.0197	529.2406	529.2471	-0.0065
	-	-	-	156.0768	156.0856	-0.0088
Sample 7	844.3836	844.4272	-0.0436	642.3246	642.3661	-0.0415
	-	-	-	413.2031	413.2082	-0.0051
Sample 16	844.3836	844.3892	-0.0056	529.2406	529.2471	-0.0065
	845.3859	845.3915	-0.0056	642.3246	642.3108	+0.0138
	846.3883	846.3945	-0.0063	689.3141	689.3146	-0.0005
	847.3906	847.3979	-0.0073	156.0768	156.0802	-0.0034
	-	-	-	826.3730	826.3615	+0.0115
	-	-	-	413.2031	413.2082	-0.0051
	-	-	-	432.1878	432.1870	+0.0008
	-	-	-	285.1194	285.1234	-0.0040
Sample 35	-	-	-	560.2715	560.2549	+0.0166
	844.3836	844.4019	-0.0183	529.2406	529.2471	-0.0065
	845.3859	845.4042	-0.0183	642.3246	642.3329	-0.0083
	846.3883	846.4072	-0.0189	156.0768	156.0802	-0.0034
	847.3906	847.3852	-0.0054	285.1194	285.1234	-0.0040
	-	-	-	413.2031	413.2082	-0.0051
	-	-	-	432.1878	432.2051	-0.0173
	-	-	-	560.2715	560.2858	-0.0143
-	-	-	689.3141	689.3261	-0.0120	

375 ¹ As determined by ‘Isotope Distribution Calculator’ (MacCoss Lab, University of Washington, USA).

376 ² Difference between theoretical and measured *m/z* values.

377 ³ As determined by ‘Fragment Ion Calculator’.

378

379 **Table 3: Overview of the multiple time regression results of BSA, Dermorphin and PapRIV using both the linear- and biphasic model (mean \pm standard**
 380 **error, 95% CI interval between brackets)**

	Peptide (¹²⁵ I-)	K _{in} ($\mu\text{L/g} \times \text{min}$)	K ₁ ($\mu\text{L/g} \times \text{min}$)	K ($\mu\text{L/g} \times \text{min}$)	Vascular Brain distribution volume, V ₀ ($\mu\text{L/g}$)	Tissue Brain distribution volume, V _g ($\mu\text{L/g}$)	Parenchym al fraction (%)	Capillary fraction (%)	k _{out} (min ⁻¹)
Linear	BSA	-0.03 \pm 0.08 [-0.23 to 0.18]	N/A	N/A	11.08 \pm 0.99 [8.62 to 13.54]	N/A	N/A	N/A	N/A
	Dermorphin	0.35 \pm 0.05 [0.23 to 0.46]	N/A	N/A	15.93 \pm 0.64 [14.38 to 17.47]	N/A	N/A	N/A	N/A
Biphasic	PapRIV	N/A	6.95 \pm 6.25 [0.00 to 22.54]	0	/†	35.70 \pm 61.73 [0.00 to 189.70]	86.92	13.08	-0.01 \pm 0.05 [-0.18 to 0.16]

381 † (V₀): The vascular brain distribution volume V₀ was set to be equal to the V₀ of radio-iodinated BSA obtained in these experiments (11.077 $\mu\text{L/g}$) (=V_i).

382 N/A: not applicable seen the model applied

383 PapRIV shows pro-inflammatory effects on BV-2 microglia cells *in vitro*

384 The PapRIV peptide showed *in vitro* pro-inflammatory effects on the microglial BV-2 cell line,
385 an immortalized murine microglial cell line which has proven its suitability for *in vitro*
386 microglial research and investigation of neuro-inflammation [55-57]. The PapRIV peptide
387 induced the production of the pro-inflammatory cytokines IL-6 and TNF α (Figure 2a); for IL-
388 6, these changes were also confirmed at the mRNA level by qPCR (Figure 2b). This induction
389 of pro-inflammatory cytokines was accompanied by an increase of intracellular ROS and an
390 increased fraction of amoeboid cells (Figure 2c-d, Supplementary Fig. S2). Treatment with 1
391 μ g/mL LPS resulted in a fraction of amoeboid cells of around \pm 50% (data not shown). This
392 microglial activation is mediated by an increased NF- κ B nuclear translocation caused by
393 decreasing I κ B α levels, an inhibitory protein of NF- κ B (Figure 2e-f). NIK expression was not
394 observed in the cells (data not shown), thus indicating a canonical activation of the NF- κ B
395 pathway [58]. By synthesizing an alanine-scan of the sequence, we could identify the crucial
396 amino acids of the peptide to exert its pro-inflammatory effects in the BV-2 microglial cells.
397 When replacing aspartic acid or proline at respectively position 2 and 4 by an alanine residue,
398 the corresponding peptide was not able anymore to induce IL-6 and TNF α production (Figure
399 2g). A scrambled control (DEHSFLP), which has the same amino acids as the native sequence
400 but arranged in a random order, also showed no activating properties indicating that the specific
401 sequence of amino acids is important for its function.

402

403 Conditioned medium of PapRIV treated BV-2 is toxic for SH-SY5Y neuroblast cells

404 Treatment of SH-SY5Y neuroblast cells with conditioned medium of BV-2 cells treated with
405 PapRIV caused toxic effects on these neuroblast cells as demonstrated by a significant
406 decreased viability of the cells (Figure 3a). This effect was not caused by direct actions of the
407 peptide itself on the neuroblast cells as a direct treatment with the peptide caused no significant

408 toxic effects (Figure 3b). The peptide thus shows indirect neurotoxic effect via microglia
409 activation.

410

411 Different metabolites of PapRIV are formed in serum, brain, liver, kidney and faeces

412 The metabolization rate of the peptide varied between different biological matrices such as
413 serum, brain tissue, liver tissue, kidney tissue and faeces. The fastest metabolization rate was
414 observed in kidney tissue, with a half-life of only 19.8 minutes. The half-lives in serum, faeces,
415 liver and brain tissue were respectively 24.8, 89.7, 286 and 523 minutes while no metabolization
416 was observed in colon tissue (Table 4, Supplementary Fig. S3). Different metabolites of the
417 peptide could be identified. To exclude the possibility of non-enzymatic degradation, the
418 chemical and protease-inactivated homogenate (by pre-heating the homogenate for 5 minutes
419 at 95°C) stability of the peptide was determined. Except for kidney tissue, PapRIV remained
420 stable in protease-inactivated homogenates, pointing an enzymatic degradation in serum, liver,
421 brain and faeces (Supplementary Table S1). In protease-inactivated kidney homogenate,
422 approximately 45% of peptide loss after 60 minutes can be explained by protein interaction
423 with some kidney specific proteins. In serum, six different metabolites were formed. The MS-
424 spectra of the different metabolites formed and the metabolic profiles in different tissues are
425 given in supplementary information (Supplementary Fig. S4-S5). DLPFEH is the main
426 metabolite which is formed in all matrices, metabolization of the native peptide to this
427 metabolite is the main contributor of the low half-lives observed in kidney tissue and serum
428 (Supplementary Fig. S5). Also in faeces, the matrix in which PapRIV is produced by gut
429 bacteria, metabolization to DLPFEH occurred. Since this peptide still contains the two critical
430 amino acids (D and P) at positions 2 and 4, respectively, the question was raised whether this
431 peptide also showed microglial activating properties. As hypothesized, DLPFEH showed
432 similar microglial activating properties as it was also able to induce IL-6 production to the same

433 extent as the native sequence; the other metabolites showed no activity (Figure 4). Remarkably,
434 SDLPF and DLPF showed no activating properties despite the presence of the two critical
435 amino acids, thereby indicating that the presence of the C-terminal EH sequence is also
436 necessary for the peptide's action.

437 **Table 4: Peptide half-lives and formed metabolites in different biological matrices**

Matrix	T _{1/2} (min)	Metabolites
Serum	24.8	DLPFEH, LPFEH, LPFE, LPF, SDLPF, DLPF
Brain	522.9	DLPFEH, LPFEH
Liver	285.7	DLPFEH, LPFEH
Kidney	19.8	DLPFEH, LPFEH
Faeces	89.7	DLPFEH
Colon	-	-

438

439 Discussion

440 PapRIV, a QSP which is produced by *Bacillus cereus*, showed *in vitro* pro-inflammatory effects
441 in BV-2 microglia cells. The peptide, which is mainly produced in the gut, is able to transfer
442 across the gastro-intestinal tract and reach the circulation based on the *in vitro* Caco-2 model.
443 A relatively low but appreciable P_{app} of $1.37 \pm 0.21 \times 10^{-9}$ cm/s is observed. A passive
444 paracellular transport mechanism is suggested, as a comparable P_{app} was observed in the
445 opposite basolateral-apical direction, as well as at 4°C (Supplementary Fig. S6). The low P_{app}
446 can be explained by the low mass balance observed (<2%), indicating that peptide is lost during
447 the experimental timeframe due to either cellular uptake or enzymatic degradation. Indeed
448 numerous brush border membrane peptidases (i.a. aminopeptidases, dipeptidylpeptidase IV)
449 are present on the apical side of the Caco-2 cells which may be responsible for enzymatic
450 degradation of PapRIV during the experimental timeframe [59, 60]. The peptide was detected
451 in 4 out of 66 mice plasma samples, while a protein BLAST search demonstrated that the
452 sequence is not present in the mouse proteome and can thus not be the result of proteolytic
453 cleavage of endogenous proteins. These findings supports the Caco-2 data that the peptide is
454 able to cross the gastro-intestinal tract and reach the circulation *in vivo*. Presence of *B. cereus*

455 in the human gastro-intestinal tract has already been demonstrated, up to 30% of vegetative
456 cells and 100% of spores can survive gastric passage [61-64]. Gut permeability is also
457 modulated by the intestinal microbiota. For example, expression of epithelial tight junction
458 proteins is downregulated by several intestinal pathogens hereby increasing the permeability of
459 the barrier [65]. The majority of *B. cereus* strains cause food poisoning and produce
460 enterotoxins which are also able to increase vascular permeability [66, 67]. Spores are able to
461 adhere in aggregates to both Caco-2 as small intestine gastro-intestinal epithelial cells which
462 triggers germination and the production of enterotoxins; bacterial cells are thus in the proximity
463 of the epithelial barrier facilitating the transport of metabolites [68]. Moreover, the intestinal
464 barrier function is affected in several gastro-intestinal disorders such as IBD, IBS, celiac disease
465 and obesity leading to a 'leaky gut' and an increased flux of luminal compounds towards the
466 circulation [65]. Also in mental disorders such as ASD, ADHD and bipolar disorder, increased
467 serum zonulin and/or claudin-5 levels are observed which is associated with respectively
468 increased intestinal and BBB permeability [69, 70].

469 Once in the circulation, the peptide can reach the blood-brain barrier where it shows a very high
470 brain influx according to the classification system of Stalmans *et al.* [54]. No significant brain
471 efflux of the peptide was observed. PapRIV is thus able to reach the brain parenchyma where
472 it can exert biological effects.

473 PapRIV showed *in vitro* microglia activating properties in BV-2 cells. A significant induction
474 of both IL-6 and TNF α , two pro-inflammatory cytokines, in these cells is observed. These
475 effects were accompanied by a significant increase of ROS. ROS are involved in the continued
476 activation of microglia, even if the activating agent is already removed, a phenomenon called
477 'reactive microgliosis' [71]. This reactive microgliosis is explained by the presence of a self-
478 amplifying loop: ROS are able to initiate NF- κ B nuclear translocation and thus induction of
479 gene transcription of pro-inflammatory mediators, while these pro-inflammatory cytokines

480 consequently can increase ROS production [72]. Whether PapRIV has a direct effect on both
481 factors or that one of both is indirectly affected by the other is yet unclear. In addition, microglia
482 are extremely plastic and undergo a variety of spatio-temporal shape changes, dependent on
483 their location and current role. Their morphology can range from highly branched, ramified
484 cells with small cell bodies to ameboid, rounded cells with large cell bodies. When microglia
485 are dormant, they have a lot of branches to survey the microenvironment; when they become
486 activated and secrete pro-inflammatory cytokines, their morphology changes to ameboid by
487 reorganizing proteins of the cell skeleton (actin, vimentin and microtubules) [73-75]. Here, an
488 increased fraction of ameboid cells was observed after PapRIV treatment which is thus an
489 additional proof of the microglia activating properties of this QSP. The effects are mediated by
490 an NF- κ B-dependent pathway, an increased nuclear translocation of NF- κ B is observed which
491 is caused by activation of the canonical pathway as a decrease of I κ B α , a cytoplasmic inhibitory
492 protein of NF- κ B, and no NIK expression (data not shown) is seen [76]. When treating SH-
493 SY5Y neuroblast cells with PapRIV conditioned BV-2 medium, toxic effects were seen at the
494 higher PapRIV concentrations. Indeed, when treating SH-SY5Y cells with conditioned medium
495 from activated BV-2 cells a decrease in viability is observed [77]. Several neurotoxic factors
496 such as pro-inflammatory cytokines and extracellular ROS have been identified which may
497 play a role in this microglia-mediated neurotoxicity [78]. Direct peptide treatment of the
498 neuroblast cells did not result in a decreased viability, indicating that the toxic effects are
499 mediated by the microglial activation. These results indicate the potential involvement of the
500 peptide in microglia-mediated neurodegeneration.

501 To investigate the structure-activity relationship of the peptide, an alanine-scan was
502 synthesized. By alternately replacing every amino acid with an alanine residue, crucial amino
503 acids of the peptide can be identified. It is demonstrated that the second (aspartic acid) and the
504 fourth (proline) amino acid are crucial for the peptide to exert its microglia activating effects.

505 A scrambled control peptide of the sequence did not show any activating effects; indicating that
 506 the specific peptide sequence is responsible for the pro-inflammatory actions.
 507 Different metabolites of the peptide were *ex vivo* identified in different tissues with DLPFEH
 508 being the main metabolite which is formed in all tissues (serum, brain, liver, kidney and faeces).
 509 This metabolite contains the two critical amino acids and our experiment demonstrated that it
 510 remains active, thus contributing to PapRIV-mediated microglial activation. Two other
 511 metabolites, i.e. SDLPF and DLPF which are formed in serum, also contain the two critical
 512 amino acids, but are no longer active. This indicates that presence of the carboxy-terminal EH
 513 sequence is also necessary for the peptide's actions. The half-live of the peptide varies from 20
 514 minutes in kidney tissue to 523 minutes in brain tissue. In serum, a half-live of 25 minutes is
 515 observed. The differences observed between the tissues are due to the high concentration of
 516 proteases in serum and the renal brush border membrane, while in colon tissue, a much lower
 517 expression of brush border enzymes is observed [79]. Using PeptideCutter and PROSPER, an
 518 *in silico* prediction of the potential responsible proteases for the observed metabolites was made
 519 [80]. DLPFEH can be formed by cleavage of Asp-N endopeptidases at position 1 and DLPF
 520 due to an extra cleavage at position 5 by chymotrypsin or proteinase K. SDLPF can be formed
 521 by actions of chymotrypsin or proteinase K at position 5, while LPFE can be formed by the
 522 simultaneous action of formic acid at position 2 and glutamyl endopeptidase or matrix-
 523 metalloprotease 9 (MMP 9) at position 6. Finally, LPF can be formed directly by the combined
 524 actions of formic acid and proteinase K or chymotrypsin (Table 5).

525 **Table 5: Overview of cleavage sites and *in silico* predicted responsible proteases**

Matrix	Cleavage sites	Proteases
Serum	S D LPF E H	Asp-N endopeptidase, formic acid, chymotrypsin, proteinase K, glutamyl endopeptidase, MMP 9
Liver	S D LPFEH	Asp-N endopeptidase, formic acid
Brain	S D LPFEH	Asp-N endopeptidase, formic acid
Kidney	S D LPF E H	Asp-N endopeptidase, formic acid, chymotrypsin, proteinase K
Faeces	S DLPFEH	Asp-N endopeptidase

526

527 **Conclusion**

528 PapRIV, a QSP produced by members of the *Bacillus cereus* group, shows *in vitro* activating
529 properties towards BV-2 microglia cells. This QSP is produced in the gut and is able to cross
530 the Caco-2 intestinal cell model via passive paracellular diffusion. Once reaching the
531 circulation, it is able to cross the blood-brain barrier and reach the brain parenchyma. Presence
532 of this QSP in mouse plasma was demonstrated for the first time. The peptide induces the
533 expression of pro-inflammatory cytokines (IL-6 and TNF α) and ROS, and increases the fraction
534 of amoeboid cells via an NF- κ B-dependent pathway in BV-2 microglia cells. Treatment of SH-
535 SY5Y neuroblast cells with PapRIV conditioned BV-2 medium results in a decreased viability
536 of these neuroblastoma cells, indicating indirect microglia-mediated neurotoxic effects of the
537 peptide.

538 Overall, our *in vitro* obtained findings indicate for the first time a possible role of these bacterial
539 quorum sensing peptides in gut-to-brain signaling, opening new avenues investigating their
540 translational relevance.

541 **References**

- 542 [1] Miller MB & Bassler BL. Quorum sensing in bacteria. *Annu Rev Microbiol.* 2001;55:165-99.
543 [2] Albuquerque P & Casadevall A. Quorum sensing in fungi--a review. *Med Mycol.* 2012;50(4):
544 337-45.
545 [3] Yashiroda Y & Yoshida M. Intraspecies cell-cell communication in yeast. *FEMS Yeast Res.*
546 2019;19(7).
547 [4] Debunne N, Verbeke F, Janssens Y, Wynendaele E & De Spiegeleer B. Chromatography of
548 Quorum Sensing Peptides: An Important Functional Class of the Bacterial Peptidome.
549 *Chromatographia.* 2018;81(1): 25-40.
550 [5] Papenfort K & Bassler BL. Quorum sensing signal-response systems in Gram-negative bacteria.
551 *Nat Rev Microbiol.* 2019;14(9): 576-88.
552 [6] Verbeke F, De Craemer S, Debunne N, Janssens Y, Wynendaele E, Van de Wiele C & De
553 Spiegeleer B. Peptides as Quorum Sensing Molecules: Measurement Techniques and Obtained
554 Levels In vitro and In vivo. *Front Neurosci.* 2017;11:183.
555 [7] Herzog R, Peschek N, Frohlich KS, Schumacher K & Papenfort K. Three autoinducer molecules
556 act in concert to control virulence gene expression in *Vibrio cholerae*. *Nucleic Acids Res.*
557 2019;47(6): 3171-83.
558 [8] Pesci EC, Milbank JB, Pearson JP, McKnight S, Kende AS, Greenberg EP & Iglewski BH.
559 Quinolone signaling in the cell-to-cell communication system of *Pseudomonas aeruginosa*.
560 *Proc Natl Acad Sci U S A.* 1999;96(20): 11229-34.

- 561 [9] Wynendaele E, Bronselaer A, Nielandt J, D'Hondt M, Stalmans S, Bracke N, Verbeke F, Van De
562 Wiele C, De Tre G & De Spiegeleer B. Quorumpeps database: chemical space, microbial origin
563 and functionality of quorum sensing peptides. *Nucleic Acids Res.* 2013;41(Database issue):
564 D655-9.
- 565 [10] De Spiegeleer B, Verbeke F, D'Hondt M, Hendrix A, Van De Wiele C, Burvenich C, Peremans K,
566 De Wever O, Bracke M & Wynendaele E. The quorum sensing peptides PhrG, CSP and EDF
567 promote angiogenesis and invasion of breast cancer cells in vitro. *PLoS One.* 2015;10(3):
568 e0119471.
- 569 [11] Wynendaele E, Verbeke F, D'Hondt M, Hendrix A, Van De Wiele C, Burvenich C, Peremans K,
570 De Wever O, Bracke M & De Spiegeleer B. Crosstalk between the microbiome and cancer cells
571 by quorum sensing peptides. *Peptides.* 2015;6440-8.
- 572 [12] Pundir P, Liu R, Vasavda C, Serhan N, Limjunyawong N, Yee R, Zhan Y, Dong X, Wu X, Zhang Y,
573 *et al.* A Connective Tissue Mast-Cell-Specific Receptor Detects Bacterial Quorum-Sensing
574 Molecules and Mediates Antibacterial Immunity. *Cell Host Microbe.* 2019;26(1): 114-22 e8.
- 575 [13] De Spiegeleer A, Elewaut D, Van Den Noortgate N, Janssens Y, Debunne N, Van Langenhove S,
576 Govindarajan S, De Spiegeleer B & Wynendaele E. Quorum sensing molecules as a novel
577 microbial factor impacting muscle cells. *Biochim Biophys Acta Mol Basis Dis.* 2020;1866(3):
578 165646.
- 579 [14] Wynendaele E, Verbeke F, Stalmans S, Gevaert B, Janssens Y, Van De Wiele C, Peremans K,
580 Burvenich C & De Spiegeleer B. Quorum Sensing Peptides Selectively Penetrate the Blood-
581 Brain Barrier. *PLoS One.* 2015;10(11): e0142071.
- 582 [15] Janssens Y, Wynendaele E, Verbeke F, Debunne N, Gevaert B, Audenaert K, Van DeWiele C &
583 De Spiegeleer B. Screening of quorum sensing peptides for biological effects in neuronal cells.
584 *Peptides.* 2018;101150-6.
- 585 [16] Barichella M, Severgnini M, Cilia R, Cassani E, Bolliri C, Caronni S, Ferri V, Canello R, Ceccarani
586 C, Faierman S, *et al.* Unraveling gut microbiota in Parkinson's disease and atypical
587 parkinsonism. *Mov Disord.* 2019;34(3): 396-405.
- 588 [17] Janssens Y, Nielandt J, Bronselaer A, Debunne N, Verbeke F, Wynendaele E, Van Immerseel F,
589 Vandewynckel YP, De Tre G & De Spiegeleer B. Disbiome database: linking the microbiome to
590 disease. *BMC Microbiol.* 2018;18(1): 50.
- 591 [18] Strati F, Cavalieri D, Albanese D, De Felice C, Donati C, Hayek J, Jousson O, Leoncini S, Renzi D,
592 Calabro A, *et al.* New evidences on the altered gut microbiota in autism spectrum disorders.
593 *Microbiome.* 2017;5(1): 24.
- 594 [19] Vogt NM, Kerby RL, Dill-McFarland KA, Harding SJ, Merluzzi AP, Johnson SC, Carlsson CM,
595 Asthana S, Zetterberg H, Blennow K, *et al.* Gut microbiome alterations in Alzheimer's disease.
596 *Sci Rep.* 2017;7(1): 13537.
- 597 [20] Xu R, Wu B, Liang J, He F, Gu W, Li K, Luo Y, Chen J, Gao Y, Wu Z, *et al.* Altered gut microbiota
598 and mucosal immunity in patients with schizophrenia. *Brain Behav Immun.* 2019.
- 599 [21] Chen JJ, He S, Fang L, Wang B, Bai SJ, Xie J, Zhou CJ, Wang W & Xie P. Age-specific differential
600 changes on gut microbiota composition in patients with major depressive disorder. *Aging.*
601 2020;12(3): 2764-76.
- 602 [22] Panza F, Lozupone M, Solfrizzi V, Watling M & Imbimbo BP. Time to test antibacterial therapy
603 in Alzheimer's disease. *Brain.* 2019;142(10): 2905-29.
- 604 [23] Valles-Colomer M, Falony G, Darzi Y, Tigchelaar EF, Wang J, Tito RY, Schiweck C, Kurilshikov A,
605 Joossens M, Wijmenga C, *et al.* The neuroactive potential of the human gut microbiota in
606 quality of life and depression. *Nat Microbiol.* 2019;4(4): 623-32.
- 607 [24] Zhu F, Ju Y, Wang W, Wang Q, Guo R, Ma Q, Sun Q, Fan Y, Xie Y, Yang Z, *et al.* Metagenome-
608 wide association of gut microbiome features for schizophrenia. *Nat Commun.* 2020;11(1):
609 1612.
- 610 [25] Sampson TR, Debelius JW, Thron T, Janssen S, Shastri GG, Ilhan ZE, Challis C, Schretter CE,
611 Rocha S, Gradinaru V, *et al.* Gut Microbiota Regulate Motor Deficits and Neuroinflammation
612 in a Model of Parkinson's Disease. *Cell.* 2016;167(6): 1469-80 e12.

- 613 [26] Shen H, Guan Q, Zhang X, Yuan C, Tan Z, Zhai L, Hao Y, Gu Y & Han C. New mechanism of
614 neuroinflammation in Alzheimer's disease: The activation of NLRP3 inflammasome mediated
615 by gut microbiota. *Prog Neuropsychopharmacol Biol Psychiatry*. 2020;100109884.
- 616 [27] Tengeler AC, Dam SA, Wiesmann M, Naaijen J, van Bodegom M, Belzer C, Dederen PJ, Verweij
617 V, Franke B, Kozicz T, *et al*. Gut microbiota from persons with attention-deficit/hyperactivity
618 disorder affects the brain in mice. *Microbiome*. 2020;8(1): 44.
- 619 [28] Kim MS, Kim Y, Choi H, Kim W, Park S, Lee D, Kim DK, Kim HJ, Choi H, Hyun DW, *et al*. Transfer
620 of a healthy microbiota reduces amyloid and tau pathology in an Alzheimer's disease animal
621 model. *Gut*. 2020;69(2): 283-94.
- 622 [29] Dinan TG & Cryan JF. The Microbiome-Gut-Brain Axis in Health and Disease. *Gastroenterol Clin
623 North Am*. 2017;46(1): 77-89.
- 624 [30] Cryan JF, O'Riordan KJ, Cowan CSM, Sandhu KV, Bastiaanssen TFS, Boehme M, Codagnone MG,
625 Cussotto S, Fulling C, Golubeva AV, *et al*. The Microbiota-Gut-Brain Axis. *Physiol Rev*.
626 2019;99(4): 1877-2013.
- 627 [31] Lach G, Schellekens H, Dinan TG & Cryan JF. Anxiety, Depression, and the Microbiome: A Role
628 for Gut Peptides. *Neurotherapeutics*. 2018;15(1): 36-59.
- 629 [32] Abdel-Haq R, Schlachetzki JCM, Glass CK & Mazmanian SK. Microbiome-microglia connections
630 via the gut-brain axis. *J Exp Med*. 2019;216(1): 41-59.
- 631 [33] Chu F, Shi M, Zheng C, Shen D, Zhu J, Zheng X & Cui L. The roles of macrophages and microglia
632 in multiple sclerosis and experimental autoimmune encephalomyelitis. *J Neuroimmunol*.
633 2018;3181-7.
- 634 [34] Geloso MC, Corvino V, Marchese E, Serrano A, Michetti F & D'Ambrosi N. The Dual Role of
635 Microglia in ALS: Mechanisms and Therapeutic Approaches. *Front Aging Neurosci*. 2017;9242.
- 636 [35] Koyama R & Ikegaya Y. Microglia in the pathogenesis of autism spectrum disorders. *Neurosci
637 Res*. 2015;1001-5.
- 638 [36] Xiang Z, Haroutunian V, Ho L, Purohit D & Pasinetti GM. Microglia activation in the brain as
639 inflammatory biomarker of Alzheimer's disease neuropathology and clinical dementia. *Dis
640 Markers*. 2006;22(1-2): 95-102.
- 641 [37] Yin Z, Raj D, Saiepour N, Van Dam D, Brouwer N, Holtman IR, Eggen BJL, Moller T, Tamm JA,
642 Abdourahman A, *et al*. Immune hyperreactivity of Abeta plaque-associated microglia in
643 Alzheimer's disease. *Neurobiol Aging*. 2017;55115-22.
- 644 [38] Erny D, Hrabe de Angelis AL, Jaitin D, Wieghofer P, Staszewski O, David E, Keren-Shaul H,
645 Mahlakoiv T, Jakobshagen K, Buch T, *et al*. Host microbiota constantly control maturation and
646 function of microglia in the CNS. *Nat Neurosci*. 2015;18(7): 965-77.
- 647 [39] Wang X, Sun G, Feng T, Zhang J, Huang X, Wang T, Xie Z, Chu X, Yang J, Wang H, *et al*. Sodium
648 oligomannate therapeutically remodels gut microbiota and suppresses gut bacterial amino
649 acids-shaped neuroinflammation to inhibit Alzheimer's disease progression. *Cell Res*.
650 2019;29(10): 787-803.
- 651 [40] Ceuppens S, Boon N & Uyttendaele M. Diversity of *Bacillus cereus* group strains is reflected in
652 their broad range of pathogenicity and diverse ecological lifestyles. *FEMS Microbiol Ecol*.
653 2013;84(3): 433-50.
- 654 [41] Bouillaut L, Perchat S, Arold S, Zorrilla S, Slamti L, Henry C, Gohar M, Declerck N & Lereclus D.
655 Molecular basis for group-specific activation of the virulence regulator PlcR by PapR
656 heptapeptides. *Nucleic Acids Res*. 2008;36(11): 3791-801.
- 657 [42] Pomerantsev AP, Pomerantseva OM, Camp AS, Mukkamala R, Goldman S & Leppla SH. PapR
658 peptide maturation: role of the NprB protease in *Bacillus cereus* 569 PlcR/PapR global gene
659 regulation. *FEMS Immunol Med Microbiol*. 2009;55(3): 361-77.
- 660 [43] Slamti L & Lereclus D. A cell-cell signaling peptide activates the PlcR virulence regulon in
661 bacteria of the *Bacillus cereus* group. *Embo j*. 2002;21(17): 4550-9.
- 662 [44] Grenha R, Slamti L, Nicaise M, Refes Y, Lereclus D & Nessler S. Structural basis for the activation
663 mechanism of the PlcR virulence regulator by the quorum-sensing signal peptide PapR. *Proc
664 Natl Acad Sci U S A*. 2013;110(3): 1047-52.

- 665 [45] Srinivasan B, Kolli AR, Esch MB, Abaci HE, Shuler ML & Hickman JJ. TEER measurement
666 techniques for in vitro barrier model systems. *J Lab Autom.* 2015;20(2): 107-26.
- 667 [46] Verbeke F, Bracke N, Debunne N, Wynendaele E & De Spiegeleer B. LC-MS Compatible
668 Antiadsorption Diluent for Peptide Analysis. *Anal Chem.* 2020;92(2): 1712-9.
- 669 [47] Mitrevski BS, Wilairat P & Marriott PJ. Evaluation of World Anti-Doping Agency criteria for
670 anabolic agent analysis by using comprehensive two-dimensional gas chromatography-mass
671 spectrometry. *Anal Bioanal Chem.* 2010;396(7): 2503-11.
- 672 [48] Janssens Y, Verbeke F, Debunne N, Wynendaele E, Peremans K & De Spiegeleer B. Analysis of
673 iodinated quorum sensing peptides by LC-UV/ESI ion trap mass spectrometry. *J Pharm Anal.*
674 2018;8(1): 69-74.
- 675 [49] Gutierrez EG, Banks WA & Kastin AJ. Murine tumor necrosis factor alpha is transported from
676 blood to brain in the mouse. *J Neuroimmunol.* 1993;47(2): 169-76.
- 677 [50] Triguero D, Buciak J & Pardridge WM. Capillary depletion method for quantification of blood-
678 brain barrier transport of circulating peptides and plasma proteins. *J Neurochem.* 1990;54(6):
679 1882-8.
- 680 [51] Banks WA & Kastin AJ. Quantifying carrier-mediated transport of peptides from the brain to
681 the blood. *Methods Enzymol.* 1989;168:652-60.
- 682 [52] Andersen CL, Jensen JL & Orntoft TF. Normalization of real-time quantitative reverse
683 transcription-PCR data: a model-based variance estimation approach to identify genes suited
684 for normalization, applied to bladder and colon cancer data sets. *Cancer Res.* 2004;64(15):
685 5245-50.
- 686 [53] Vandesompele J, De Preter K, Pattyn F, Poppe B, Van Roy N, De Paepe A & Speleman F.
687 Accurate normalization of real-time quantitative RT-PCR data by geometric averaging of
688 multiple internal control genes. *Genome Biol.* 2002;3(7).
- 689 [54] Stalmans S, Gevaert B, Wynendaele E, Nielandt J, De Tre G, Peremans K, Burvenich C & De
690 Spiegeleer B. Classification of Peptides According to their Blood-Brain Barrier Influx. *Protein*
691 *Pept Lett.* 2015;22(9): 768-75.
- 692 [55] Blasi E, Barluzzi R, Bocchini V, Mazzolla R & Bistoni F. Immortalization of murine microglial cells
693 by a v-raf/v-myc carrying retrovirus. *J Neuroimmunol.* 1990;27(2-3): 229-37.
- 694 [56] Henn A, Lund S, Hedtjarn M, Schrattenholz A, Porzgen P & Leist M. The suitability of BV2 cells
695 as alternative model system for primary microglia cultures or for animal experiments
696 examining brain inflammation. *ALTEX.* 2009;26(2): 83-94.
- 697 [57] Timmerman R, Burm SM & Bajramovic JJ. An Overview of in vitro Methods to Study Microglia.
698 *Front Cell Neurosci.* 2018;12(242).
- 699 [58] Shih RH, Wang CY & Yang CM. NF-kappaB Signaling Pathways in Neurological Inflammation: A
700 Mini Review. *Front Mol Neurosci.* 2015;877.
- 701 [59] Brewis IA, Howell S, Hooper NM, Kenny AJ & Turner AJ. Membrane peptidase expression by
702 confluent cultures of Caco-2 cells. *Biochem Soc Trans.* 1993;21 (Pt 3)(3): 252s.
- 703 [60] Howell S, Brewis IA, Hooper NM, Kenny AJ & Turner AJ. Mosaic expression of membrane
704 peptidases by confluent cultures of Caco-2 cells. *FEBS Lett.* 1993;317(1-2): 109-12.
- 705 [61] Ceuppens S, Uyttendaele M, Drieskens K, Rajkovic A, Boon N & Wiele TV. Survival of *Bacillus*
706 *cereus* vegetative cells and spores during in vitro simulation of gastric passage. *J Food Prot.*
707 2012;75(4): 690-4.
- 708 [62] Ceuppens S, Van de Wiele T, Rajkovic A, Ferrer-Cabaceran T, Heyndrickx M, Boon N &
709 Uyttendaele M. Impact of intestinal microbiota and gastrointestinal conditions on the in vitro
710 survival and growth of *Bacillus cereus*. *Int J Food Microbiol.* 2012;155(3): 241-6.
- 711 [63] Tam NK, Uyen NQ, Hong HA, Duc le H, Hoa TT, Serra CR, Henriques AO & Cutting SM. The
712 intestinal life cycle of *Bacillus subtilis* and close relatives. *J Bacteriol.* 2006;188(7): 2692-700.
- 713 [64] Turnbull PC & Kramer JM. Intestinal carriage of *Bacillus cereus*: faecal isolation studies in three
714 population groups. *The Journal of hygiene.* 1985;95(3): 629-38.

- 715 [65] Bischoff SC, Barbara G, Buurman W, Ockhuizen T, Schulzke JD, Serino M, Tilg H, Watson A &
716 Wells JM. Intestinal permeability--a new target for disease prevention and therapy. *BMC*
717 *Gastroenterol.* 2014;14:189.
- 718 [66] Moravek M, Dietrich R, Buerk C, Broussolle V, Guinebretière M-H, Granum PE, Nguyen-the C
719 & Märklbauer E. Determination of the toxic potential of *Bacillus cereus* isolates by quantitative
720 enterotoxin analyses. *FEMS Microbiol Lett.* 2006;257(2): 293-8.
- 721 [67] Shinagawa K, Ueno S, Konuma H, Matsusaka N & Sugii S. Purification and characterization of
722 the vascular permeability factor produced by *Bacillus cereus*. *The Journal of veterinary medical*
723 *science.* 1991;53(2): 281-6.
- 724 [68] Bottone EJ. *Bacillus cereus*, a volatile human pathogen. *Clin Microbiol Rev.* 2010;23(2): 382-
725 98.
- 726 [69] Asbjornsdottir B, Snorraddottir H, Andresdottir E, Fasano A, Lauth B, Gudmundsson LS,
727 Gottfredsson M, Halldorsson TI & Birgisdottir BE. Zonulin-Dependent Intestinal Permeability in
728 Children Diagnosed with Mental Disorders: A Systematic Review and Meta-Analysis. *Nutrients.*
729 2020;12(7).
- 730 [70] Kiliç F, Işık Ü, Demirdağ A, Doğuç DK & Bozkurt M. Serum zonulin and claudin-5 levels in
731 patients with bipolar disorder. *J Affect Disord.* 2020;266:37-42.
- 732 [71] Bordt EA & Polster BM. NADPH oxidase- and mitochondria-derived reactive oxygen species in
733 proinflammatory microglial activation: a bipartisan affair? *Free Radic Biol Med.* 2014;76:34-46.
- 734 [72] Yang D, Elner SG, Bian ZM, Till GO, Petty HR & Elner VM. Pro-inflammatory cytokines increase
735 reactive oxygen species through mitochondria and NADPH oxidase in cultured RPE cells. *Exp*
736 *Eye Res.* 2007;85(4): 462-72.
- 737 [73] Abd-el-Basset E & Fedoroff S. Effect of bacterial wall lipopolysaccharide (LPS) on morphology,
738 motility, and cytoskeletal organization of microglia in cultures. *J Neurosci Res.* 1995;41(2): 222-
739 37.
- 740 [74] Colton C & Wilcock DM. Assessing activation states in microglia. *CNS Neurol Disord Drug*
741 *Targets.* 2010;9(2): 174-91.
- 742 [75] McHugh D, Roskowski D, Xie S & Bradshaw HB. Delta(9)-THC and N-arachidonoyl glycine
743 regulate BV-2 microglial morphology and cytokine release plasticity: implications for signaling
744 at GPR18. *Front Pharmacol.* 2014;4:162.
- 745 [76] Moynagh PN. The NF-kappaB pathway. *J Cell Sci.* 2005;118(Pt 20): 4589-92.
- 746 [77] Kwon SJ, Ahn TB, Yoon MY & Jeon BS. BV-2 stimulation by lactacystin results in a strong
747 inflammatory reaction and apoptotic neuronal death in SH-SY5Y cells. *Brain Res.*
748 2008;1205:116-21.
- 749 [78] Block ML & Hong JS. Microglia and inflammation-mediated neurodegeneration: multiple
750 triggers with a common mechanism. *Prog Neurobiol.* 2005;76(2): 77-98.
- 751 [79] Darmoul D, Voisin T, Couvineau A, Rouyer-Fessard C, Salomon R, Wang Y, Swallow DM &
752 Laburthe M. Regional expression of epithelial dipeptidyl peptidase IV in the human intestines.
753 *Biochem Biophys Res Commun.* 1994;203(2): 1224-9.
- 754 [80] Song J, Tan H, Perry AJ, Akutsu T, Webb GI, Whisstock JC & Pike RN. PROSPER: an integrated
755 feature-based tool for predicting protease substrate cleavage sites. *PloS one.* 2012;7(11):
756 e50300.

757

758 **Declarations**

759 **Competing interests**

760 The authors declare that they have no competing interests.

761 **Funding**

762 ND and ADS are supported by a grant of Research Foundation Flanders (FWO) (grant numbers
763 1S21017N and 1158818N respectively). Part of this work was financed by grant
764 MPCUdG2016/038 from the University of Girona. The funding bodies have no role in writing
765 the manuscript.

766 **Acknowledgements**

767 We thank Professor Alba Minelli for the kind gift of BV-2 cells.

768 **Authors' contributions**

769 YJ, ADS, ND and EW performed the experiments. MP and LF performed the synthesis of the
770 alanine-scan and metabolites. AQ and CC performed the iPSC experiments. YJ, ND, ADS and
771 BDS analyzed data. YJ, EW, DVD, PDD, PP, MBJ and BDS designed the experiments. YJ and
772 BDS wrote the manuscript. The authors read and approved the final manuscript.

773 **Availability of data and material**

774 The datasets used and/or analysed during the current study are available from the corresponding
775 author on reasonable request.

776 **Ethics approval and consent to participate**

777 Not applicable

778 **Consent for publication**

779 Not applicable

780 **List of Abbreviations**

781 QSP = Quorum sensing peptide

782 ICR-CD-1 = Institute for Cancer Research, Caesarean Derived-1

783 BBB = Blood-brain barrier

- 784 ASD = Autism spectrum disorder
- 785 AD = Alzheimer's disease
- 786 PD = Parkinson's disease
- 787 ROS = Reactive oxygen species
- 788 FBS = Fetal bovine serum
- 789 NEAA = Non-essential amino acids
- 790 TMB = Tetramethylbenzidine
- 791 SEM = Standard error on mean
- 792 MMP-9 = Matrix-metalloprotease 9
- 793

794 **Figure legends**

795 Figure 1: PapRIV passes the Caco-2 monolayer and blood-brain barrier. (a) The PapRIV peptide passes
796 the Caco-2 monolayer and accumulates in the acceptor compartment (n = 6). (b) Multiple time regression
797 analysis of BSA, Dermorphin and PapRIV across the blood-brain barrier. BSA and Dermorphin, the
798 negative and positive controls respectively, follow a linear model while the PapRIV peptide is following
799 a biphasic model with an initial steep influx followed by a steady state. (c) After 10 minutes, 87% of the
800 peptide reaches the brain parenchyma while 13% remains in the capillaries (n = 2). (d) Efflux data of
801 the peptide from the brain to the circulation.

802

803 Figure 2: *In vitro* microglial activation of BV-2 cells by PapRIV. (a) IL-6 and TNF α levels increase
804 after increasing concentrations of PapRIV (n = 6). (b) IL-6 mRNA expression is increased after
805 treatment with 10 μ M PapRIV (n = 6). *** = p<0.001 (Mann-Whitney U test) (c) Reactive oxygen
806 species are formed after treatment (n = 12). (d) The fraction of amoeboid cells, a marker for microglial
807 activation, increased after treatment (n = 6). (e-f) Activation is mediated by an increased nuclear
808 translocation of NF- κ B caused by decreasing I κ B α levels (n = 3). (g) Critical amino acids are identified
809 by an alanine scan of the native sequence (10 μ M, n = 12). Mean \pm SEM, One-way ANOVA, post-hoc
810 Dunnett.

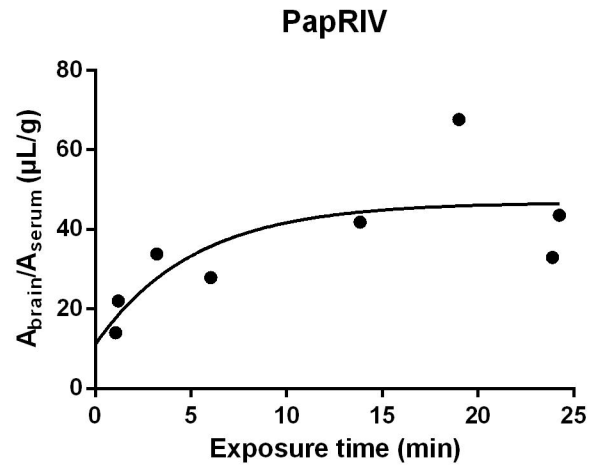
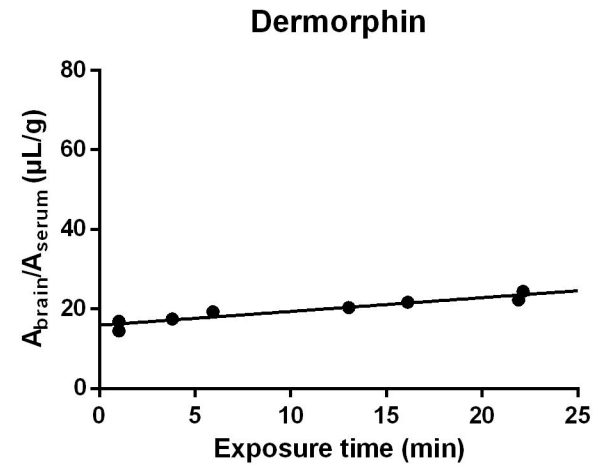
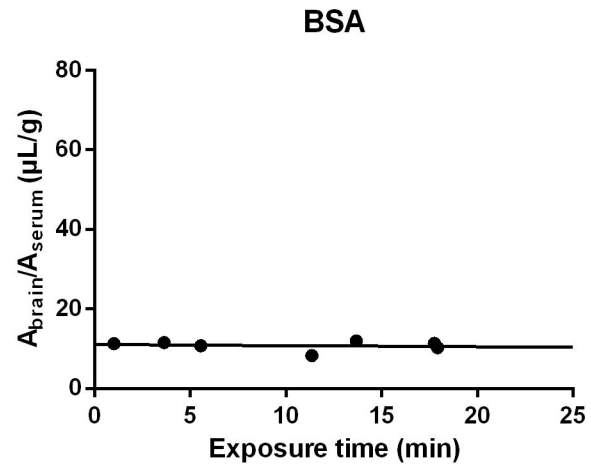
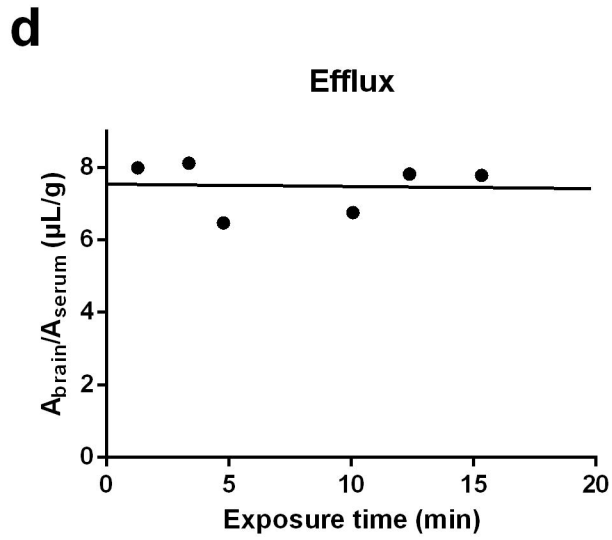
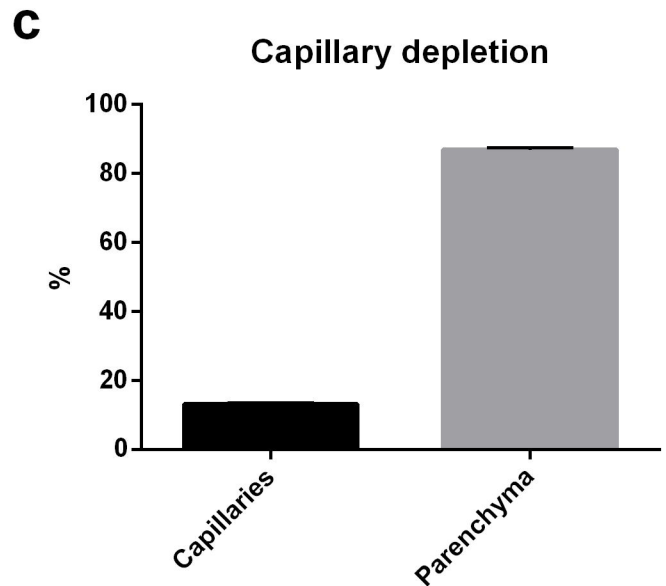
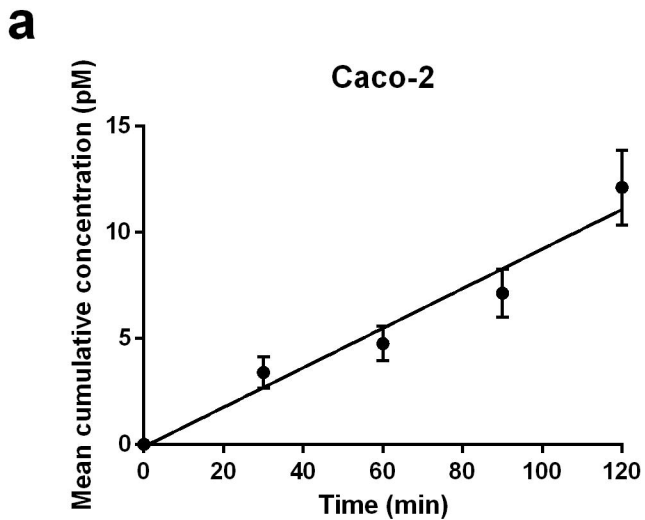
811

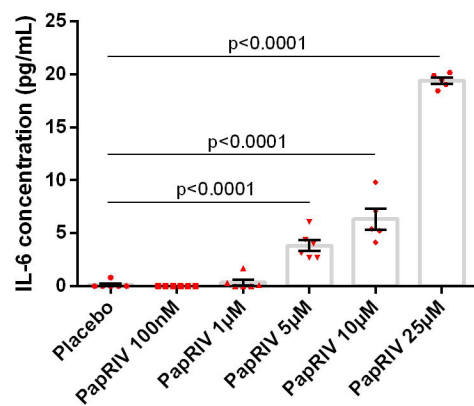
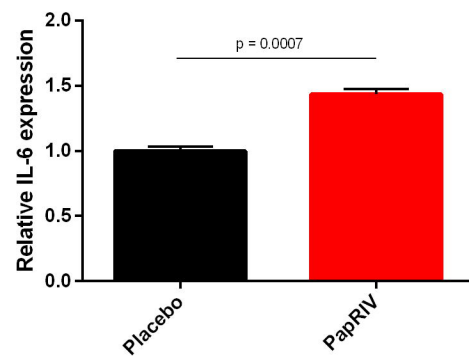
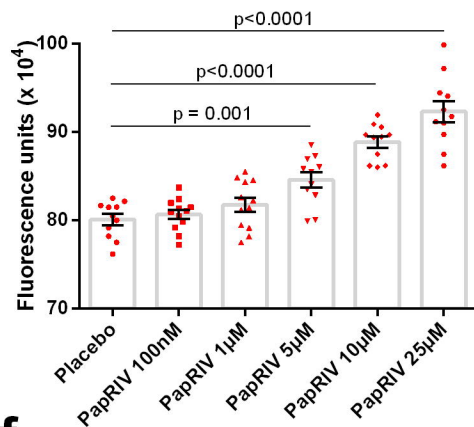
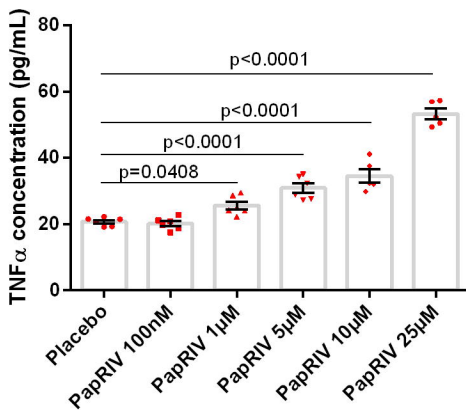
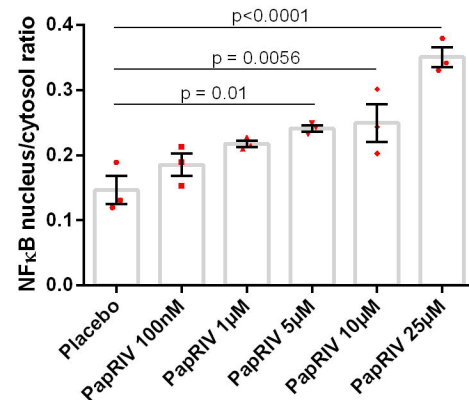
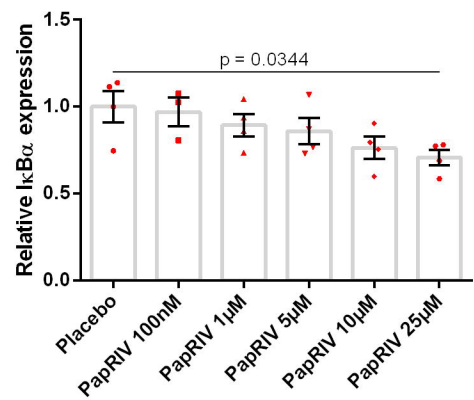
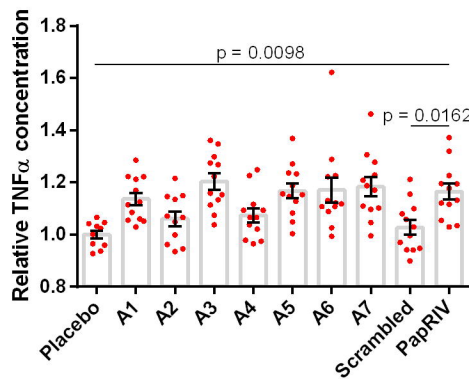
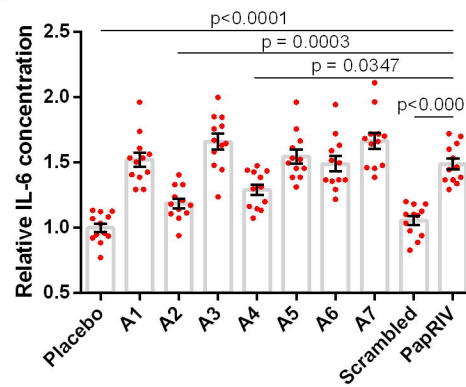
812 Figure 3: Indirect neurotoxic effects of PapRIV via microglia activation. (a) Treatment of SH-SY5Y
813 cells with conditioned medium of PapRIV peptide-treated BV-2 cells is toxic for these neuroblasts (n =
814 6). (b) Direct treatment of SH-SY5Y cells with PapRIV shows no direct toxicity (n = 6). Mean \pm SEM,
815 one-way ANOVA, post-hoc Dunnett.

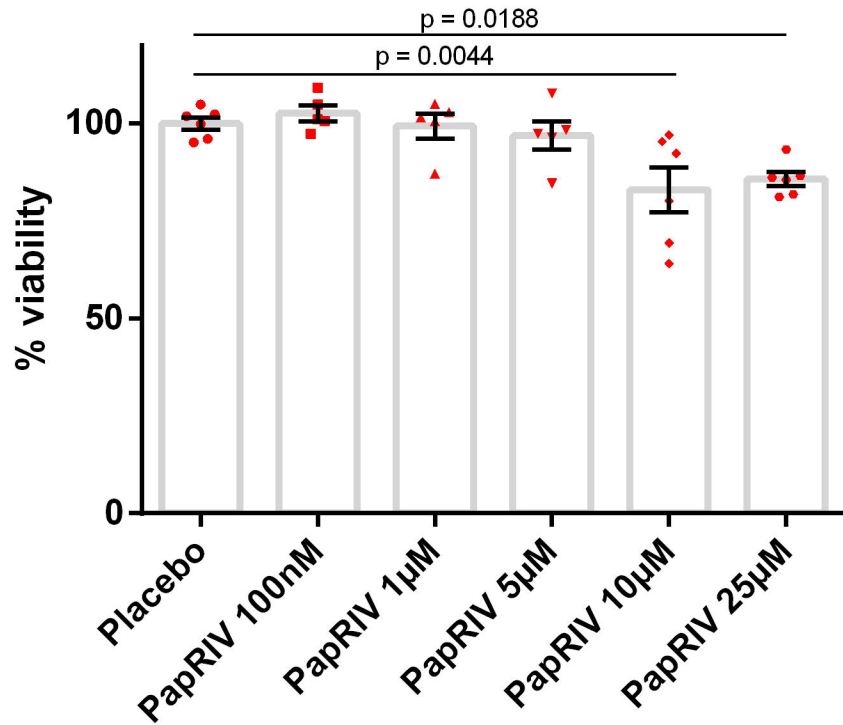
816

817 Figure 4: Activating properties of PapRIV metabolites on BV-2 microglia cells (10 μ M, n = 12). Mean
818 \pm SEM, one-way ANOVA, post-hoc Dunnett.

819



a**b****c****d****e****f****g**

a**BV-2 conditioned medium****b****PapRIV**